Spline wavelet packets application: Doppler signal analysis during operation time

E. SERRANO, R.O. SIRNE, M. FABIO, A. VIEGENER,
C.E. D'ATTELLIS and J. GUGLIELMONE
Escuela Superior Ténica del Ejército "Gral. M.N. Savio"
Universidad de Palermo - Fac. de Ingeniería
Cabildo 15, (1426) Buenos Aires
ARGENTINA
eserrano@unsam.edu.ar, ceda@favaloro.edu.ar

Abstract: - Wavelet methods play a significant role in signal processing. They are multifaceted tools and many choices and alternatives are open. Particularly, the Discrete Transform leads us to decompose the given signal in a filter bank, or time scale-scheme called multiresolution analysis. Then, the wavelet coefficients reflect the signal information in an efficient structure. Wavelet packets, in a second and deeper analysis, refine the scheme and they give us more frequency precision. In this article, we applied these techniques in a spline framework to process Doppler radar signals. Over-the-horizon-Radars operate in the High Frequency band; they are able to detect targets beyond the horizon and are employed in many applications. The radar operates for long periods of time without interruption; this requires analyzing the echo signal during the time of operation. For this case, we propose an adaptation of Mallat's algorithm; the method compute the wavelet's coefficients of consecutive intervals of the signal in a multiresolution analysis framework. The coefficients are calculated and used efficiently to estimate the radial velocity of the target over the time.

Key-Words:- Wavelets, wavelet packet, multiresolution, spline, radar, signal segmentation.

1 Introduction

High Frequency (HF) radio frequencies (RF) are between 3 and 30 MHz, with wavelengths between 100 to 10 meters respectively. The HF band are extensively used for medium and long-range communications, taking advantage of the reflection (really, total refraction) of the waves in the ionosphere.

Over-the-horizon-Radars (OTHRs) operates in the High Frequency band ([8], [16]). They are able to detect targets beyond the horizon and are employed in many applications such as scientific meteorological studies, surveillance and oceanic platform control. Some OTHRs utilize the electromagnetic waves' reflection in the ionosphere while others operate in a surface wave propagation mode (ground wave).

A moving target reflects radars transmitted signal s_t of frequency ν_t , producing a radar return signal s_r of frequency ν_r. The frequency shift

$$\nu_0 = |\nu_r - \nu_t| \tag{1}$$

is proportional to the radial velocity V of the target with respect to the source of radiation (Doppler effect). When the target is moving towards the radar, the frequency ν_r of the echo signal is higher than the emitted frequency ν_t. Conversely, if the target is moving away from the radar, ν_r is lower than ν_t.

Then, the relative radial velocity V can in this way be estimated by measuring ν_0, this frequency is the beat note obtained when the receiver mixes s_r with s_t and passes the output trough a lowpass filter during the continuous wave (CW) emission mode of the radar.

Wavelets play a significant role in applied mathematics when time-scale methods are required, or it performs better than Fourier methods. The Discrete Wavelet Transform is correlated with orthonormal wavelet bases and a multiresolution scheme ([3], [4]). It gives us a discrete

spectra of filtered versions of the signal resulting from its convolutions with the analyzing wavelet, well localized both in time and frequency domain.

A non trivial problem is to choice the orthogonal analyzing wavelet. Compactly supported wavelet are proposed in [4]. Spline functions are a nice alternative ([3], [19]). Spline orthogonal wavelets are symmetric, have exponential decay and are well localized on the frequency domain. Particularly, cubic spline is efficient and kindly elemental function for numerical applications.

The wavelet coefficients can be recursively computed with the Mallat's algorithm, using a pair of conjugate filters, [3]. Here we propose some variation in these filters exploiting the spline properties and given some numerical and computational advantages, [11].

Moreover, we implement a method to calculate these coefficients during the operation time. In this way, they can be used efficiently to estimate the radial velocity on line with the radar operation.

We use the following notation:

t	:	time.
Δt	:	sampling rate interval.
$\tau = t/\Delta t$	:	normalized time, with t and Δt in the same unit (e.g.: sec.).
ν	:	frequency.
$\nu_s = 1/\Delta t$	:	sampling rate frequency.
$f = \nu/\nu_s$	:	normalized frequency, with ν and ν_s in the same unit (e.g.: Hz).

In the following section briefly we expound on the relationship between V and ν_0.

2 CW mode operation

Assuming that the radar is rest at the origin in the space, and the transmitting antenna converts the signal emitted $s_t(t)$ to a full electromagnetic wave, this wave $u(X,t)$ satisfy the equation

$$\frac{1}{c^2}u_{tt}(X,t) - \nabla^2 u(X,t) = s_t(t)\delta(X) \qquad (2)$$

where $X = (x,y,z)$ is the position vector, t is the time, δ is the Dirac-delta, c is the constant propagation speed of the light, and $\nabla^2 u = u_{xx} + u_{yy} + u_{zz}$.

The electromagnetic wave is reflected from a target, and the receiving antenna converts the echo to the receiving signal s_r.

If both antennas are at the origin space and the target (essentially a point) moves directly toward or away from the radar at a constant velocity V, the distance (range) varies with time according to

$$r(t) = r_0 + Vt \qquad (3)$$

where $r = (x^2+y^2+z^2)^{1/2}$, then it can be demonstrated ([6],[7]) that the received signal is

$$s_r(t) = A(r)\, s_t(\sigma t - t_0) \qquad (4)$$

where $A(r) \cong A_0/r_0^2$ is the attenuation factor with A_0 constant and t_0/σ is a delay time.

The time scaling factor

$$\sigma = \frac{c-V}{c+V} \qquad (5)$$

represent the Doppler effect where $\sigma > 0$, c is the speed of light and

$$t_0 = \frac{2\ r_0}{c+V}. \qquad (6)$$

The objective consists on estimating V; for details, the cited bibliography has been proposed. As we mentioned in the Introduction, the frequency of the beat note ν_0 is proportional to V.

The analogical procedure to obtained the beat note in the receiver can be represented by the lowpass filter of the signal

$$s_B(t) = s_t\ s_r(t). \qquad (7)$$

This procedure is particularly suitable in case that the emitted signal is sinusoidal; if

$$s_t(t) = \mathrm{sen}(2\pi\nu_t t) \qquad (8)$$

where ν_t is the emission frequency, then

$$s_B(t) = \tfrac{A_0}{2r_0^2}[\cos(2\pi\nu_t(1-\sigma)t + 2\pi\nu_t t_0) - \\ - \cos(2\pi\nu_t(1+\sigma)t - 2\pi\nu_t t_0)] \qquad (9)$$

where $s_B(t)$ is the sum of two monochrome waves associated to the frequencies

$$\nu_0 = \nu_t\,|1-\sigma| \ \text{ and } \ \nu_1 = \nu_t\,(1+\sigma). \qquad (10)$$

Since $\sigma \cong 1$, see Eq. (5) with $|V| << c$, these frequencies are very different. The filtering operations allows to separate the contribution of the

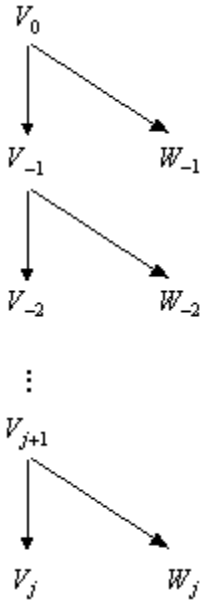

Figure 1: Multiresolution scheme.

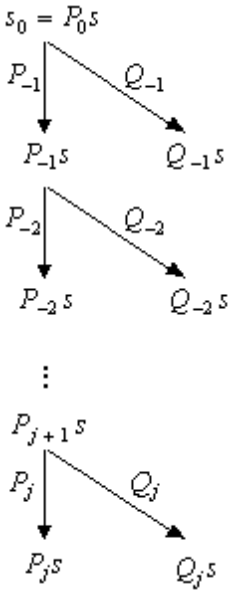

Figure 2: Signal projections.

high frequency, to specify the low frequency and to estimate ν_0. Using (5), result

$$V = c\ \frac{1-\sigma}{1+\sigma} \cong c\,(1-\sigma)/2. \qquad (11)$$

Therewith and ν_0 as per (10), we obtained

$$|V| \cong \frac{c\,\nu_0}{2\,\nu_t}. \qquad (12)$$

Knowing ν_0 and assuming $c = 3\ 10^8$ m/sec, with (12) we can estimate $|V|$ ([14],[15]) with relative error less than $1.9\ 10^{-4}$ for velocities less than 100 Km/h.

The precision of the obtained V value will depend on the frequency approach; in this sense, the convenience of detecting ν_0 using an appropriate bandpass filter, with adjustable range, it suggests the employment of wavelets. The cubic spline orthogonal wavelets ([19]), in a multiresolution analysis context, allows us to approach ν_0 in a range or band, associated to certain scale or resolution level ([10],[20]); finally, the approach is obtained from the wavelet coefficients of this level using appropriate Fourier matrices ([13]).

3 Multiresolution analysis

A multiresolution analysis of $L^2(\mathbb{R})$ ([4],[10]) consists on a collection of nested subspaces $V_j,\ j \in \mathbb{Z}$ such that:

- $V_j \subset V_{j+1}$
- $\bigcap_{j\in\mathbb{Z}} V_j = \{0\}$ and $\bigcup_{j\in\mathbb{Z}} V_j$ is dense in $L^2(\mathbb{R})$
- $s(\tau) \in V_j \Leftrightarrow s(2\tau) \in V_{j+1}$
- $s(\tau) \in V_0 \Leftrightarrow s(\tau - n) \in V_0\ ,\ n \in \mathbb{Z}$
- There exists a scaling function $\phi \in V_0$ such that the family $\{\phi(\tau - k), k \in \mathbb{Z}\}$ is an orthonormal basis of V_0.

Let W_j be the orthogonal complement of V_j in V_{j+1}:

$$V_{j+1} = V_j \oplus W_j \ \text{ and } \ V_j \perp W_j \qquad (13)$$

and let $P_j s$ and $Q_j s$ the orthogonal projections of the signal s on Vj and W_j respectively. Then

$$P_{j+1}s = P_j s + Q_j s\ , \qquad (14)$$

particularly:

$$P_0 s = \sum_{j=-\infty}^{-1} Q_j s. \qquad (15)$$

Figure 1 shows the multiresolution scheme; the orthogonal projections are depicted in Fig. 2.

On the other hand there is a second function

$$\psi \in W_0 \subset V_1\ , \qquad (16)$$

called *mother wavelet*, such that the family

$$\{\psi(\tau - k),\ \ k \in \mathbb{Z}\} \qquad (17)$$

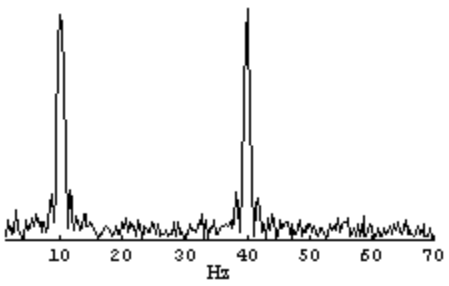

Figure 3: Spectra of signal s_0, see text.

is an orthogonal basis of W_0.

In correspondence, the full family

$$\{\psi_{j,k}(\tau) = 2^{j/2}\psi(2^j\tau - k), \quad j,k \in \mathbb{Z}\} \qquad (18)$$

is an orthonomal basis of $L^2(\mathbb{R})$ and

$$Q_j s(\tau) = \sum_{k=-\infty}^{\infty} < s, \psi_{j,k} > \psi_{j,k}(\tau). \qquad (19)$$

Figure 3 shows the spectra of a signal $s_0 \in V_0$ sampled with $\nu_s = 200$ Hz, it has two principal components of 10 and 40 Hz in differents time interval and aditive noise.

That signal and its projections $\sigma_j = Q_j s \in W_j$ with $j = -1, \cdots, -6$ are depicted in Fig. 4.

We observe that each $Q_j s$ represent the time-localization of the frequency contain of the signal in different frequency band, these band will be defined in Section 5.

4 Algorithm implementation

Among several alternatives we choice orthogonal cubic spline wavelets. At it is well known these functions defining a suitable framework for signals and image processing ([3], [19]).

Particularly, cubic spline lead us to apply and develop efficient numerical methods to represent and analyze a given signal in the multiresolution scheme.

Let $V_0 \subset L^2(\mathbb{R})$ the space of cubic spline functions with integer knots. That is, they are twice differentiable and then agree with cubic polynomials in each interval $[k, k+1]$. It generate a multiresolution analysis ([3], [4]).

Let $\psi(\tau)$ the associated orthogonal cubic spline wavelet (OCS). It is a function with knots in the half integers $k/2, k \in \mathbb{Z}$.

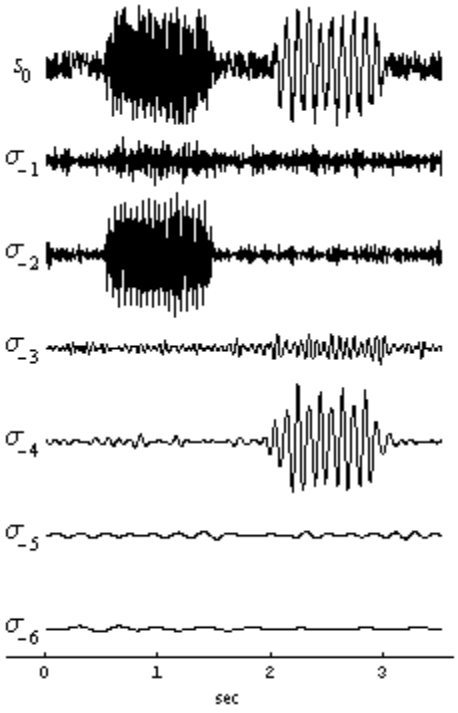

Figure 4: $Q_j s = \sigma_j$ are the projections of s_0.

Denote

$$s_j[k] = P_j s(2^{-j}k) \qquad (20)$$

the sampled values of the signals projections on V_j, and

$$d_j[k] =< s, \psi_{j,k} > \qquad (21)$$

the wavelet coefficients.

Assuming that $s \in V_0$, we must to compute these values per $j = -1, -2, \cdots$.

For these purposes we recall the cardinal cubic spline function $L \in V_0$, verifying

$$L(n) = \begin{cases} 1 & \text{if} \quad n = 0 \\ 0 & \text{if} \quad n \in \mathbb{Z}, n \neq 0 \end{cases} \qquad (22)$$

Then we can write

$$P_j s(\tau) = \sum_{n=-\infty}^{\infty} s_j[n]\ L(2^j\tau - n) \qquad (23)$$

Next we define the discrete filter

$$g[n] = 2^{-1/2} \int_{-\infty}^{\infty} L(\tau - n)\ \psi(\tau/2)\ d\tau \qquad (24)$$

for each $n \in \mathbb{Z}$ and we remark that it has exponential decay ([19]).

Then

$$< L(2^{j+1} \cdot -n)\ , \psi_{j,k} >= 2^{-j/2} g[n - 2k] \qquad (25)$$

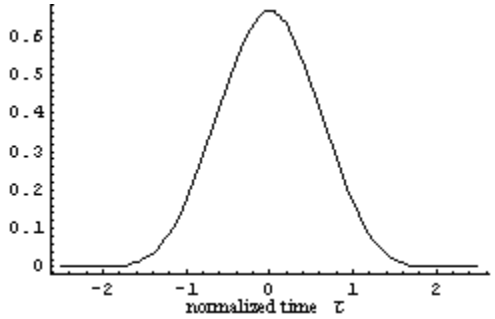

Figure 5: Basic Spline M_3.

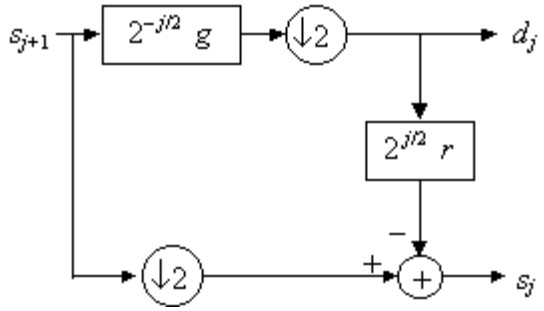

Figure 6: Computing scheme.

for each $j \in \mathbb{Z}$, $k \in \mathbb{Z}$.

Following, we compute the wavelet coefficients

$$\begin{aligned} d_j[k] &= < s, \psi_{j,k} > = < P_{j+1}s, \psi_{j,k} > \\ &= \sum s_{j+1}[n] \ < L(2^{j+1}\tau - n), \psi_{j,k} > \\ &= 2^{-j/2} \sum s_{j+1}[n] \ g[n-2k] \\ &= 2^{-j/2}(s_{j+1} \star g)[2k]. \end{aligned} \tag{26}$$

On the other hand, we have

$$P_j s(\tau) = P_{j+1}s(\tau) - Q_j s(\tau) \tag{27}$$

that is

$$P_j s(2^{-j}n) = P_{j+1}s(2^{-j}n) - Q_j s(2^{-j}n) \tag{28}$$

but

$$Q_j s(2^{-j}n) = 2^{j/2} \sum_{k=-\infty}^{\infty} d_j[n] \ \psi(n-k). \tag{29}$$

Then

$$s_j[n] = s_{j+1}[2n] - 2^{j/2}(d_j \star r)[n] \tag{30}$$

where

$$r[n] = \psi(n). \tag{31}$$

We sumarize: given the sampled data

$$s_0[0], \ \cdots \ , s_0[2^n - 1]$$

for $j = -1, \cdots, -N$

$$\begin{aligned} d_j[n] &= 2^{-j/2}(s_{j+1} \star g)[2n] \\ &= 2^{-j/2}(s_{j+1} \star g)_{\downarrow 2}[n] \end{aligned} \tag{32}$$

where $a_{\downarrow 2}[n] = a[2n]$, and

$$s_j[n] = (s_{j+1})_{\downarrow 2}[n] - 2^{j/2}(d_j \star r)[n] \tag{33}$$

as shows Fig.6.

Next, recall that the Basic Spline function or Schorenbergs central B-Spline ([19]) is defined as:

$$\begin{aligned} M_0(\tau) &= \chi_{[-1/2,1/2)}(\tau) \\ M_{\eta+1}(\tau) &= M_\eta \star M_0 \ (\tau) \end{aligned} \tag{34}$$

where

$$\chi_{[-1/2,1/2)}(\tau) = \begin{cases} 1 & \text{if } -1/2 \le \tau < 1/2 \\ 0 & \text{, otherwise} \end{cases} \tag{35}$$

is the characteristic function in the interval $[-1/2, 1/2)$.

Particularly, depicted in Fig. 5, the function

$$M_3(\tau) = \begin{cases} (2+\tau)^3/6 & \text{if } -2 \le \tau < -1 \\ \frac{1}{6}(4 + 3|\tau|^3 - 6\tau^2) & \text{if } |\tau| \le 1 \\ (2-\tau)^3/6 & \text{if } 1 < \tau \le 2 \\ 0 & \text{if } |\tau| > 2 \end{cases} \tag{36}$$

is the convolution of four characteristics functions and the family

$$\{M_3(\tau - n), n \in \mathbb{Z}\} \tag{37}$$

is a Riesz basis for the fundamental subspace V_0.

Also we remark that:

$$M_3 \star M_3(\tau) = M_7(\tau) \tag{38}$$

then,

$$< M_3(\tau - n), M_3(\tau - m) > = M_7(m - n) \tag{39}$$

Moreover, M_3 is supported on $[-2, 2]$ and the filter $M_7[k]$ is finite (FIR).

Denote ϕ and ψ the scaling function and wavelet corresponding to the orthogonal cubic spline multiresolution scheme, since

$$\phi, \psi \in V_1 \subset V_0$$

we can write

$$\phi(\tau/2) = \sum_m p[m]\ M_3(\tau - m). \qquad (40)$$

and

$$\psi(\tau/2) = \sum_m h[m]\ M_3(\tau - m), \qquad (41)$$

the coefficients $p[m]$ and $h[m]$ can be computed using the methods and formulas given in [3] and [19].

It follows that

$$r[m] = \sum_n h[n] M_3(2m - n). \qquad (42)$$

We also can write ([11])

$$L(\tau) = \sum_n l[n] M_3(\tau - n) \qquad (43)$$

where

$$l[n] = \sqrt{3}\ (\sqrt{3} - 2)^{|n|}\ , n \in \mathbb{Z}. \qquad (44)$$

Then we can conclude that the filter g, as defined in (24), is given by the bilinear form

$$g[n] = 2^{-1/2} \sum_k \sum_m l[k]\ h[m]\ M_7(m - k - n). \qquad (45)$$

Since h and l have exponential decay and M_7 has finite support, these filters r and g can be efficientely computed and aproximated by finite filters ([11]).

5 Frequency characterization

Denote $u(t)$ a signal and the time t, we define

$$s(\tau) = u(\tau\ \Delta t), \qquad (46)$$

the sampling values of s for $\tau = n \in \mathbb{Z}$ are the sampling of u for each Δt.

That is

$$\{s(n),\ n \in \mathbb{Z}\} = \{u(n\ \Delta t),\ n \in \mathbb{Z}\}. \qquad (47)$$

On the other hand, the Fourier transform of s is

$$\hat{s}(f) = \int_{-\infty}^{\infty} u(\tau\ \Delta t)\ e^{i2\pi f \tau} d\tau \qquad (48)$$

and, with $\tau = \nu_s t$, result:

$$\hat{s}(f) = \nu_s\ \hat{u}(\nu_s f). \qquad (49)$$

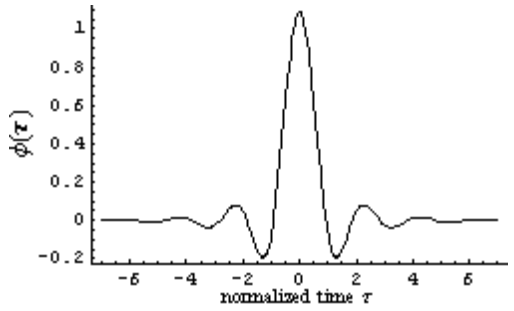

Figure 7: OCS–scaling function ϕ.

Then, all normalized frequency f of the $s(\tau)$ spectra is in correspondence with the frequency

$$\nu = \nu_s\ f \qquad (50)$$

of the $u(t)$ spectra.

Using the orthogonal cubic splines, the scale function ϕ depicted in Fig. 7 has a behavior like an almost ideal lowpass filter with cutoff frequency 0.5; Fig. 8 shows the module of the frecuency response of ϕ.

Then, we observe that the spectra of $s(\tau) \in V_0$ (that is, $s_0(\tau)$) contains normalizad frequencies $f \leq 0.5$; in correspondence with (50) and the spectra of the signal $u_0(t)$ vanishes for frequencies $\nu > \nu_s/2$.

Figure 10 shows the module of the frequency response of $\psi(\tau)$, that is the wavelet acts as a passband filter localized in $[0.5, 1]$ and the functions $\psi_{j,k} \in W_j$ as (18) act as passband filters with bandpass $[0.5\ 2^j, 2^j]$

According to (50), the wavelet coefficients $d_j[k] =< s, \psi_{j,k} >$ corresponding to $Q_j s(\tau) \in W_j$, give us the information of the signal $u(t)$ in the frequency band:

$$[2^{j-1}\nu_s\ ,\ 2^j \nu_s]. \qquad (51)$$

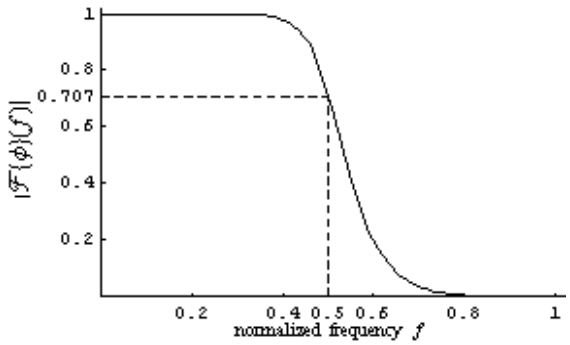

Figure 8: OCS–lowpass filter with scaling function.

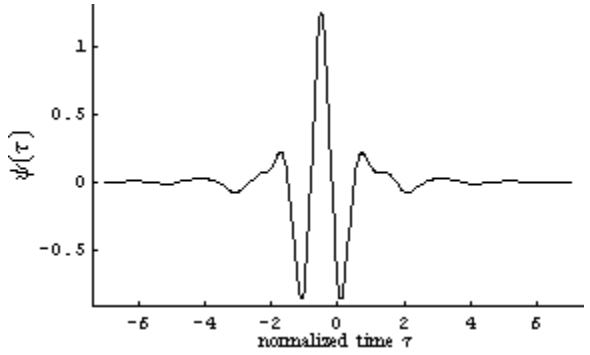

Figure 9: Orthogonal cubic spline (OCS) wavelet.

6 Spline wavelet packets

Let $\psi(\tau)$ the orthogonal cubic spline (OCS) wavelet depicted in Fig.9 and

$$\hat{\psi}(f) = |\hat{\psi}(f)|e^{-i\pi f} \tag{52}$$

its Fourier transform ([3]).

As we mentioned in the last section $\hat{\psi}(f)$ is a bandpass filter on $1/2 \leq |f| \leq 1$, but it is not localized at any frequency; that is, the module of the frequency response $|\mathcal{F}\ (\psi)(f)| \equiv |\hat{\psi}(f)|$ is almost constant on the bandpass, this is illustrated in Fig.10 for $f > 0$.

Then the wavelet transform gives us a time-scale representation rather than a time-frequency one. To over come this disadvantage we have proposed in [15] a new family of spline wavelet packets.

For this purposes, given $N = 2^p$ a fixed parameter called *size block*, we define the frequencies

$$f_n = \begin{cases} 1 + n/N & \text{if} \quad 1 - N/2 \leq n \leq 0 \\ n/N - 1 & \text{if} \quad 1 \leq n \leq N/2 \end{cases} \quad ; \tag{53}$$

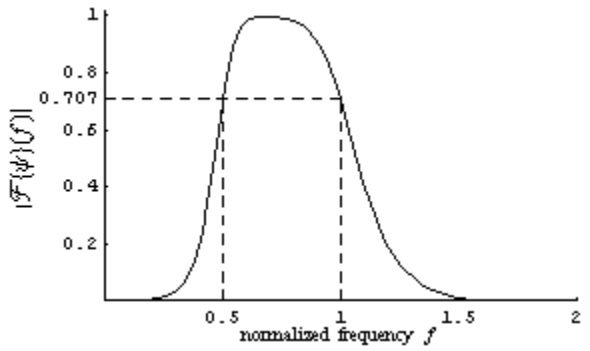

Figure 10: OCS-bandpass filter.

localized on $1/2 \leq |f_n| \leq 1$.

Defining the Fourier matrices

$$e_{N,n} = \left(\frac{1}{\sqrt{N}} e^{-i\pi f_n (2k+1)} \right)_{0 \leq k < N} \tag{54}$$

with $1 - N/2 \leq n \leq N/2$, the family $e_{N,n}$ is an orthogonal basis of $\mathcal{C}^{\mathcal{N}}$.

The wavelet packets are defined in W_0 as

$$\Theta_{N,n}(\tau) = \sum_{k=0}^{N-1} e_{N,n}[k]\ \psi(\tau - k) \tag{55}$$

for $1 - N/2 \leq n \leq N/2$; then the family

$$\{\Theta_{N,n}(\tau - b\ N),\ 1 - \frac{N}{2} \leq n \leq \frac{N}{2}, b \in \mathbb{Z}\} \tag{56}$$

is an orthogonal basis of the subspace W_0. The extension to other subspaces W_j is analogous.

If $d_j[k]$ mentioned in (26) are the wavelet coefficients for a given signal, the orthogonal wavelet packet transform in W_j is defined as

$$w_{j,n}[r] = \sum_{k=0}^{N-1} e_{N,n}[k]\ d_j[k] \tag{57}$$

for real signals, the values $|w_{j,n}[r]|^2 + |w_{j,-n}[r]|^2$ represent the local contribution of the frequency $2^j|f_n|$. We refer to [15] for details.

We only need N entries (the size block) $d_j[k]$ to compute the values $w_{j,n}[r]$ for each r. Then we can identify $N/2$ frequencies $2^j|f_n|$.

This suggests an efficient procedure to optimize the memory used in the computational implementation.

7 Method description

With a constant size block $N = 2^p$ and assuming that $s \in V_0$, we denotes for $j = 0$, $k = 0, 1, 2, \cdots$:

$$S_0(k) = (\ s_0[k\ 2^p], \cdots, s_0[(k+1)\ 2^p - 1]\ ) \tag{58}$$

where $s_0[\ \cdot\ ]$ are the values of the sampled signal; and for $j \leq -1$:

$$S_j(k) = (\ s_j[k\ 2^p], \cdots, s_j[(k+1)\ 2^p - 1]\ ) \tag{59}$$

$$D_j(k) = (\ d_j[k\ 2^p], \cdots, d_j[(k+1)\ 2^p - 1]\ ) \tag{60}$$

all these vectors have $N = 2^p$ entries.

For each pair $(S_{j+1}(2n), S_{j+1}(2n+1))$ it is possible to compute the vectors $D_j(n)$ and $S_j(n)$ as showed in Fig. 11, where:

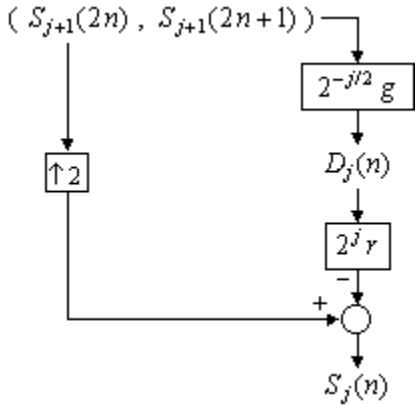

Figure 11: Computing method of $D_j(n)$ and $S_j(n)$.

$D_j(n)$: is analized with wavelet packets and erased from memory.

$$\xi_{\uparrow 2}(r) = \begin{cases} \xi(k) & \text{for } r = 2k, k \in \mathbb{Z} \\ 0 & \text{otherwise} \end{cases}$$

$S_j(n)$: is stored in memory until the next iteration, erasing $S_{j+1}(2n)$ and $S_{j+1}(2n+1)$.

The block generation is ordered as follows:

$$(\mathrm{O}_1) \quad : \quad S_j(n) < S_j(n+1)$$
$$(\mathrm{O}_2) \quad : \quad S_j(2n+1) < S_{j-1}(n) < S_j(2n+2)$$

the iterative process is depicted in Fig.12, it begins computing $S_0(0)$ and $S_0(1)$ to obtained $S_{-1}(0)$; the last one is stored in memory until it can be used with $S_{-1}(1)$ to obtained $S_{-2}(0)$.

Then, it is necessary to store in memory the N entries of the vector $S_j(2n)$ until to can computed $S_{j-1}(n)$ using the pair $(S_j(2n), S_j(2n+1))$.

Since r and g are IIR filters with exponential decay, in practice we implement appropriated finite version of them, see [15] and [19] for details.

8 Application

We apply the proposed method to obtain the radial velocity of a target detected by a radar; this

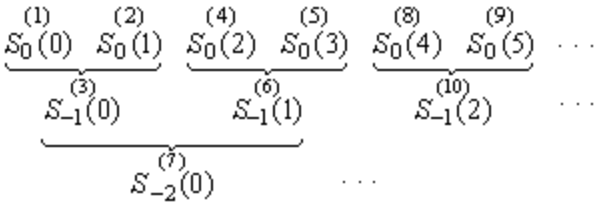

Figure 12: Order generation blocks $S_j(n)$.

velocity V is around 20 km/hour or 5.56 m/sec.

The signal was provided by a Doppler radar with an emission frequency $\nu_t = 10^{10}$ Hz. Then, knowing ν_0 and assuming $c = 3\,10^8$ m/sec, with (12) we can estimate $|v|$ in Km/h using

$$|v| \cong 0.054\,\nu_0\ , \tag{61}$$

or

$$|v| \cong 0.015\,\nu_0\ , \tag{62}$$

in m/sec.

We analyze the beat signal obtained in the audio frequency band, digitalized with a sampling frequency $\nu_s = 44100$ Hz through a 16-bit A/D converter.

Since we can assume that the target velocity is bounded by $V \le V_{max} = 10$ m/sec, the associated frequency ν_0 must be bounded by $\nu_{max} = 667$ Hz.

We analyze the signal in the multiresolution scheme, for levels $j = -1, -2, \ldots$; we remark that –see (51)– each level j is associated with the frequency band $[\ 2^{j-1}\nu_s\ ,\ 2^j\nu_s\ ]$.

Table 1 shows for each resolution level, the frequency bands

$$[\ 2^{j-1}\nu_s\ ,\ 2^j\nu_s\ ]\ ,\quad j = -1, \cdots, -10$$

and the corresponding –using (61)– velocity intervals

$$[\ 0.054\,2^{j-1}\nu_s\ ,\ 0.054\,2^j\nu_s\ ]\ ,\quad j = -1, \cdots, -10.$$

level	**frequency**		**velocity**	
j	Hz		Km/h	
$\cdots$	min	max	min	max
-1	11025.00	22050.00	595.35	1190.70
-2	5512.50	11025.00	297.68	5953.50
-3	2756.25	5512.50	148.34	297.68
-4	1378.13	2756.25	74.42	148.84
-5	689.06	1378.13	37.21	74.42
-6	344.53	689.06	18.60	37.21
-7	172.27	344.53	9.30	18.60
-8	86.13	172.27	4.65	9.30
-9	43.07	86.13	2.33	4.65
-10	21.53	43.07	1.16	2.33

Table 1: Frequency bands and velocity intervals for each multiresolution level j.

For these reasons we will search the frequency ν_0 in the rank $j \le -6$. Computing the energy

$$E_j = \sum_k |d_j[k]|^2 \tag{63}$$

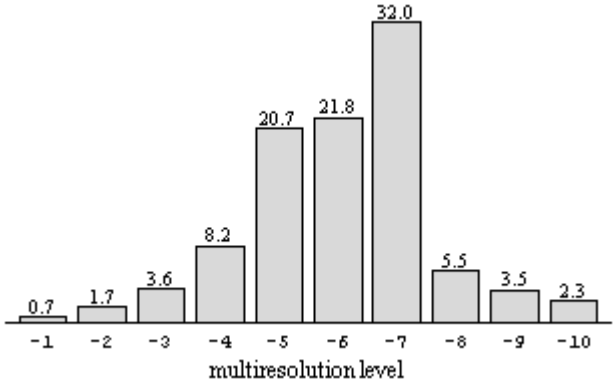

Figure 13: Percent energy distribution.

and the percent energy distribution

$$PE_j = 100\frac{E_j}{E_T} \quad \text{with} \quad E_T = \sum_{j=-1}^{-10} E_j. \qquad (64)$$

Computing PE_j during a signal interval of three blocks of 2048 values ($\cong$ 46.44 mseg), we obtained the results depicted in Fig.13.

Table 2 shows the greatest values 100 E_j/E_T observed; the more important (32%) corresponds to $j = -7$, in accord with the real velocity of the car.

level	**energy**	**velocity**	
j	%	min –Km/h–	max
-4	8.2	74.42	148.84
-5	20.7	37.21	74.42
-6	21.8	18.60	37.21
-7	32.0	9.30	18.60

Table 2: Percentual values of energy.

We can see that the top energy correspond to levels $j = -6$ and $j = -7$, that suggest a variation of the target velocity during the process. Applying wavelet packets to each block we detect the greatest amplitude for the following frequencies:

355.33 Hz, 315.56 Hz and 333.46 Hz,

corresponding to the velocities

19.19 Km/h, 17.03 Km/h and 18.00 Km/h,

or

5.33 m/sec, 4.73 m/sec and 5.00 m/sec,

respectively.

These describe the velocity variations, just as before it was supposed.

9 Conclusion

Wavelet analysis is a powerful tool for signal processing, particularly for Doppler radar signals. The algorithm used is based on a multiresolution analysis with appropriated orthogonal wavelets to obtain the resolution level corresponding to the band of frequency where is included the Doppler shift; finally, this shift is estimated from the wavelet packet coefficients using Fourier matrices.

The iterative proposed process of calculation for successive intervals of the signal with fixed size blocks, is an effective procedure to optimize the amount of memory required. It can be used to perform the analysis of signal during the time of radar's operation.

Further these results, a broad way for wavelet applications in radar signal processing is open. By example, we refer to another recent correlated develops using wavelets in [2], [5], [12], [17].

Another applications of wavelet transform are in [1], [9], [18].

References

[1] Abdullah S., A. Zaharim, Using The Orthogonal Wavelet Transform to Identify Fatigue Features in Variable Amplitude Fatigue Loadings, *WSEAS Transaction of Signal Processing*, Issue 10, Vol. 2, October 2006, pp. 1416-1420.

[2] Aly O.A.M, A.S. Omar, A.Z. Elsherbeni, Detection and localization of RF radar pulses in noise environments using wavelet packect transform and higher order statistics, *Progress In Electromagnetics Research*, PIER 58, 2006, pp. 301-317.

[3] Chui C.K., *An Introduction to Wavelets*, Academic Press, 1992.

[4] Daubechies I., *Ten Lectures on Wavelets*, SIAM,1992.

[5] Fengshan L., L. Yi, X. Xiangen, S. Xiquan, Wavelets methods for ground penetrating radar imaging. *Journal of Computational and Applied Mathematics*, Vol. 169, Issue 2, 2004, pp. 459-474.

[6] Kaiser G., Phisical Wavelets and Radar - A Variational Approach to Remote Sensing, *IEEE Antennas and Propagation Magazine*, 1996.

[7] Kaiser G., *A Friendly Guide to Wavelets*, Birkhäuser, 1994.

[8] Kingsley S., S. Quegan, *Understanding Systems*, SciTech Publishing, 1999.

[9] Lara Castro O.J. , C. Castejon Sisamon, J.C. Garcia Prada, Bearing Fault Diagnosis based on Neural Network Classification and Wavelet Transform, *WSEAS Transaction of Signal Processing*, Issue 10, Vol. 2, October 2006, pp. 1371-1378.

[10] Mallat S., *A Wavelet Tour of Signal Processing*, Academic Press, 1998.

[11] Melas D., E. Serrano, Algoritmo rápido para el análisis de señales mediante onditas spline, preprint 191, *IAM-CONICET*, 1992.

[12] Ovarlez, J.P., L. Vignaud, J.C. Castelli, M. Tria, M. Benidir, Analysis of SAR images by multidimensional wavelet transform, *Radar, Sonar and Navigation, IEEE Proceedings*, Vol.150, Issue 4, 2003, pp. 234-241.

[13] Serrano E., M. Fabio, Applications of the Wavelet Transform to Acoustic Signal Processing, *IEEE Trans. Acoust., Speech and Signal Processing*, Vol.44, No.5, 1996, pp. 1270-1275.

[14] Serrano, E., R.O. Sirne, M. Fabio, A.D. Popovsky, C.E. D'Attellis, Doppler Detection in HF Radars Using Wavelets, *WSEAS Transactions on Signal Processing*, Issue 3, Vol. 2, March 2006, pp. 372-375.

[15] Serrano, E., R. Sirne, C. D'Attellis, Wavelet Packets Analysis for Doppler Effect Detection, *WSEAS Transaction of Signal Processing*, Issue 10, Vol. 2, October 2006, pp.1437-1441.

[16] Skolnick M.I., *Radar Handbook - Chapter 24:* J.M. Headrick, *HF Over-the-Horizon Radar*, McGraw-Hill, 1990.

[17] Sri Hari P., P. Rajesh Kumar P.,Tirumala Rao D., Raja Rajeswari K., Fuzzy Modelling for Discrimination and Merit Factor of Radar Coded Waveforms, *WSEAS Transactions on Signal Processing*, Issue 4, Vol. 3, April 2007, pp. 313-320.

[18] Touqir I., M. Saleem, A.M. Siddiqui, Novel Wavelet Based Edge Detection, *WSEAS Transactions on Signal Processing*, Issue 9, Vol. 2, September 2006, pp. 1248-1253.

[19] Unser M., A. Aldroubi, M. Eden, A family of polynomial spline wavelet transforms, *Signal Processing, Elsevier Science Publishers*, 30, 1993, pp. 141-162.

[20] Unser M. and T. Blu, Fractional Spline and Wavelets, *SIAM Rev.*, Vol.42, No.1, Jan 2000.